EVIREC: Efficient Visual Indexing and Retrieval for Edge Crowd-sensing

Abstract—The abundance of images in Visual crowd-sensing data makes it difficult to identify and eliminate redundant data involving manpower and handcrafted techniques. In this paper, we propose Efficient Visual Indexing and Retrieval for Edge Crowd-sensing (EVIREC) method that identifies and eliminates redundant data. EVIREC uses Deep Nural Network (DNN) to extract features from images and performs Approximate Nearest Neighbor (ANN) search to retrieve duplicate or near duplicate images in the database. Using a threshold of distance or similarity in the feature space, EVIREC can efficiently eliminate redundant images of high variability in appearance, position, and angles. The careful design of the indexing algorithm and similarity match technique ensures that duplicate detection is accurate and real-time with a minimum computational overhead. The experimental results demonstrate that EVIREC surpasses state-of-the-art hashing-based and CNN-based methods in terms of performance on the CIFAR10, CIFAR100, and Birds data sets. Moreover, to test the robustness of our proposed model, we combined the three data sets and presented the accuracy across 560 classes. EVIREC successfully eliminates redundant images with an impressive rate of up to 99.99%, making it the most robust method for the image deduplication task in visual crowd-sensing image data.

Index Terms—Data redundancy, crowd-sensing, Visual crowd-sensing, Big data, Mobile crowd-sensing, Image deduplication.

Fig. 1. Deduplication workflow for Crowd-Sensing images.

I. Introduction

The rapid development of Internet of Things (IoT) devices has led to an explosion of data being generated from various sources. This data must be stored, processed, and analyzed to extract valuable insights and make informed decisions.

One emerging paradigm addressing this challenge is Mobile crowd-sensing (MCS) [10], [26], which involves volunteers contributing data obtained by their sensor-enhanced mobile devices. MCS leverages the capabilities of smartphones and other mobile devices to collect data from the environment. It can use different sensing modalities, including audio, pictures/videos, and numeric quantities such as GPS coordinates, temperature, and air quality. Among these modalities, visual crowd-sensing (VCS) has gained popularity. visual crowd-sensing utilizes the in-built cameras of intelligent devices, enabling users to contribute to various tasks by sending images or video information from their surroundings. Compared to traditional approaches like mounting still cameras in specific locations, visual crowd-sensing provides more informative and diverse data. It allows for real-time data collection from different perspectives and locations, making it particularly useful for environmental monitoring, urban planning, and disaster management applications.
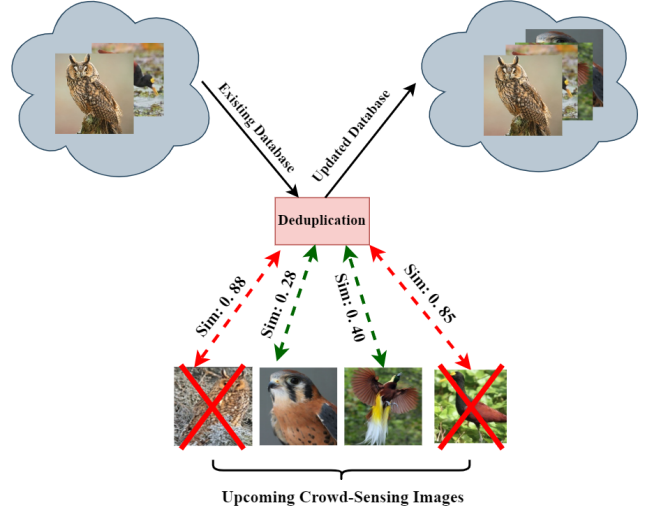
Several successful projects have been proposed based on VCS, demonstrating its potential. Examples include Creek-Watch [18], FlierMeet [8], PhotoCity [36], PhotoNet [37], WreckWatch [39], Mediascope [14]. These projects have shown that engaging a crowd of mobile device users makes it possible to gather a large volume of data from various sources, improving the coverage and accuracy of the collected information.

Visual crowd-sensing is challenging when dealing with vast images and videos. There is a high chance of redundancy in the content as multiple users capture and contribute similar or identical information. The task has evolved to semantic aggregation: the system needs an efficient way to identify and eliminate redundant content, as storage is not unlimited and search time increases with larger databases. The search for (near) identical images has posed a significant challenge with the rise in VCS's popularity as users worldwide share many images. However, a considerable portion of these uploaded images is either slightly altered or exact replicas of an original image [23]. This abundance of duplicate images in the image storage system drives up costs of storing and accessing content and negatively impacts the performance when the system searches a massive database of duplicate or near-duplicate images, drives up the storage cost and [29].

The need for crowdsensing data management arose from the storage and processing limits, and the simplest techniques

involve data deduplication. As shown in Figure 1, in the deduplication process, the redundant data is identified and stored only once, or data aggregation methods to consolidate similar information from multiple sources [10]. Recent machine learning techniques can analyze and process the data, identify patterns, extract relevant information, and summarize the crowd-sensing data. However, efficiently indexing or retrieving images from an extensive image cloud storage system proves highly challenging [17].

Therefore, there is a need for an efficient real-time or online technique that can filter out duplicates of an original image before sending it to the storage (See Figure 1), thus enhancing overall system storage efficiency. In this paper, we propose a novel approach called **E**fficient **V**isual **I**ndexing and **R**etrieval for **E**dge **C**rowd-sensing (EVIREC) to address the issue of redundant data in Visual crowd-sensing (VCS) image data. EVIREC aims to efficiently identify and eliminate duplicate or near duplicate images to the previously stored image data from the visual crowd-sensing data.

The suggested approach entails extracting and storing features from newly arrived images incrementally. These features serve as descriptive representations of the images, capturing crucial visual attributes invariant of scale, angle, and appearance. By incrementally extracting and preserving these features, we establish a database of pre-existing features and index them in a way that allows for efficient searching. This enables us to determine the similarity between an incoming image and the previously stored images.

To determine the similarity between an incoming image and the existing features in the database, we propose Hierarchical Layered Graph (HLG), an Approximate Nearest Neighbor (ANN) search to retrieve the most similar item from the feature database. ANN search is chosen over the traditional k-Nearest Neighbor (k-NN) approach because it can handle large-scale databases. ANN search is more suitable for large databases consisting of millions of images, as it can handle searching in a million-scale feature database [15], [27], [28], [31]. In contrast, k-NN becomes progressively slow when dealing with high-dimensional features and large databases [19].

After retrieving the most similar feature using the HLG search, EVIREC employs either the Euclidean distance in the feature space or the cosine similarity score to determine the similarity of an incoming image. If the incoming image is deemed sufficiently similar to the retrieved feature according to some threshold, it is classified as redundant and can be discarded. Conversely, if the image is distinctive enough, it is considered unique. Then, the feature is included in the existing feature database, and the incoming image is stored in the image database. EVIREC reduces the storage requirements and processing overhead associated with redundant data in visual crowd-sensing big data. By eliminating duplicate or near duplicate images, the data set becomes more compact and efficient, improving the overall performance of visual crowd-sensing applications. In summary, we make the following contributions-

1) We propose the EVIREC framework, which, to our

knowledge, is the first method that utilizes graph-based approximate nearest neighbor search in deep features to accomplish the image de-duplication task.

2) We propose a novel graph-based approximate nearest neighbor indexing and search method, Hierarchical Layered Graph (HLG), in an extensive deep descriptor database to efficiently retrieve the most similar image descriptor.

3) We employ normalized cosine similarity to determine whether a query image closely resembles any image in the database.

The rest of this article is organized as follows. Section II summarizes related work, and section III discusses our proposed EVIREC method and training pipeline in detail. Next, Section IV describes the experimental data set distribution and characteristics. In Section V, we evaluate the proposed framework and show our experimental results by comparing the latest deduplication benchmarks over three consumer and crowd-sensing data sets. Finally, we summarize the findings in Section VI.

II. RELATED WORK

Data selection and redundancy elimination are the critical challenges in visual crowd-sensing data [9]. Several image deduplication methods have been proposed over the past few years, which can be categorized mainly into Hashing-based [4], [34], [38], [42] and Convolutional Neural Network (CNN) based methods [17], [24].

This idea is easy and uncomplicated: If more people report an observation, it is more likely to be significant, whereas things with few observers can be viewed as outliers. Data utility or usefulness in TaskMe [7] is measured by predefined task restrictions rather than clustering findings. A photo is considered an outlier in PhotoNet [37] if it is geographically close to a famous picture cluster yet visually distinct from the group. However, lone images are sometimes relevant, and the pertinent sensing targets might be found in areas with few observers. EVIREC handles this problem by keeping the lone images if they differ in features from other images in the database. The creation of data selection strategies for visual crowd-sensing has been extensively studied. For instance, CrowdPic [6] presents a general picture collection framework that facilitates effective picture grouping and redundancy removal based on multi-dimensional job constraints. To support online crowd-sourcing photo grouping and represent the task requirements, the pyramid-tree (PTree) method is presented. Some visual crowd-sensing programs try to acquire data selection techniques from human experience or expert knowledge. The computational domain-specific filming rules in MoVieUp [40] include the 30-degree rule and the less shot-switching concept (there should be at least 30 degrees' variation between shooting angles to prevent jump cuts in camera selection). A framework called MoViMash [32] compiles video clips of an event shot from various distances and viewpoints. They used a hidden Markov model to learn from the experiences of expert
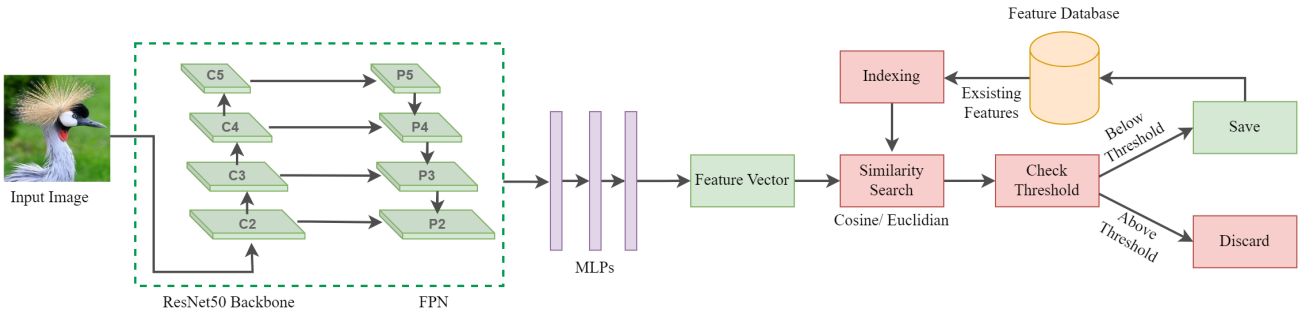
Fig. 2. Proposed EVIREC pipeline.

editors, such as choosing the shooting angle and distance, shot length, and transitions.

A. Hashing-based

Image hashing involves examining the content of an image and generating a distinct identifier based on its specific characteristics. The image is processed through a hash function, resulting in a value representing its visual properties. Similar images should produce similar hash values, and by comparing the variances in hashes, visually similar images are identified.

QHash [25] was explicitly designed for low-variance image de-duplication, which aims to minimize the occurrence of false positives and false negatives during the de-duplication process, thereby improving the overall accuracy and efficiency of image de-duplication systems. The algorithm comprises three main steps: pre-processing, feature extraction, and hash code generation. In the pre-processing step, the input image is resized and converted to grayscale for efficiency. Feature extraction involves quantization and salient point detection algorithms to capture global and local features. The hash code generation combines the extracted features with a hash function to produce the final hash code.

The AHash algorithm [4] downsamples an image to a size of N × N pixels (8 × 8 in this paper) to remove high frequencies and details. After that, the RGB image is converted to grayscale, and the average pixel value Pmean is determined. Each pixel Pval is then compared to Pmean, and a bit value Pbit of 1 is assigned if Pval is greater than Pmean; otherwise, 0. The resulting 8 × 8 binary matrix is flattened into a 64-bit integer to produce the final hash. AHash is a fast and straightforward hashing algorithm. However, directly comparing with the mean might not provide consistent outcomes.

The initial step of the Dynamic Hashing (DHash) algorithm [38] involves resizing the image to a resolution of N × (N + 1) (8 × 9 in this particular paper). After that, the RGB image is converted to grayscale. To convert the pixels into binary form, DHash examines the neighboring pixels. In detail, each pixel is assigned a value of 1 if its pixel value is greater than the pixel to its right; otherwise, it is assigned a value of 0. As a result of this process, an 8 × 8 binary matrix is created. The DHash

algorithm improves upon AHash by comparing adjacent pairs of pixels, thereby preserving more local patterns.

The Perceptual Hashing (PHash) algorithm [42] involves resizing the image to a resolution of 32 × 32 pixels. Then, the algorithm utilizes the Discrete Cosine Transform (DCT) [1] to convert the spatial RGB values into a set of frequencies and magnitudes. Only the top-left 2-dimensional matrix measuring 8 × 8 is retained to eliminate the high-frequency elements. The average value of this matrix is calculated to create a binary matrix, which is subsequently flattened into a 64-bit integer serving as the hash representation.

On the other hand, the paper [5] introduced a rapid image retrieval method that converts 128-DSIFT features into 128-bit binary representations. Hash values are computed for each feature, and the hamming distance is utilized to identify similar images. This technique significantly decreases the search retrieval time. The Wavelet Hashing (WHash) algorithm [34] shares similarities with PHash, with the key difference being its utilization of the Discrete Wavelet Transform (DWT) [33] for the conversion of spatial RGB values into frequencies and magnitudes.

B. Deep Neural Network Modeling

A deep CNN model is trained using a large data set of diverse images to learn and extract discriminative features [17]. The model is trained to map similar images to close feature representations while maintaining a significant distance for dissimilar images. During the online de-duplication phase, when a new image is uploaded to the cloud system, it undergoes a series of pre-processing steps. These steps involve resizing, normalization, and feature extraction using the pre-trained deep CNN model. The extracted features are then compared with the features of existing images in the cloud storage. To efficiently search for duplicate images, an indexing mechanism based on locality-sensitive hashing (LSH) is employed. LSH enables fast approximate nearest neighbor search, quickly identifying potential duplicates.

Cost-effective convolutional neural nets training based on image deduplication (CE-Dedup) [24] focuses on assessing the impact of near-duplicate images on CNN training performance. CE-Dedup combines a hashing-based image de-duplication approach with downstream CNN-based image

classification tasks. The framework aims to balance a high de-duplication ratio with maintaining stable accuracy. This is achieved by heuristically adjusting the de-duplication threshold. The goal of CE-Dedup is to make CNN training more cost-effective by reducing redundancy in the training data without sacrificing performance.

A technique was proposed by S. Thaiyalnayaki et al. [35] to identify near-duplicate images by utilizing the Speeded-Up Robust Feature (SURF) algorithm and the segmented minhash algorithm. The SURF algorithm is employed to extract image features, while the segmented minhash algorithm is used to index the similarity of the extracted images. Locality Sensitive Hashing is applied to index the near-duplicate images.

Kaur et al. propose a CNN-based online image deduplication technique focused on the cloud storage system [17]. The proposed Deep CNN-based method detects exact and near-exact images using cross-domains, even in perturbations due to blur, noise, compression, lighting variations, and many more external influences. In the experiments, the paper shows that the proposed deep CNN for the online image deduplication technique outperforms existing hashing methods regarding image matching accuracy and performance. A Hot Decomposition Vector (HDV) is also integrated for image patch generation to store efficiently dissimilar parts of near-exact images.

In this paper, we propose EVIREC. EVIREC handles the camera angle and orientation problem by training a DNN model with varying images in different orientations, lighting, and angles. The DNN model can capture these conditions and extract features from an image database.

III. METHODOLOGY

EVIREC works to detect and eliminate redundant images in an existing database and build a database without adding redundant images. Fig.2 shows the proposed pipeline of our EVIREC method. There are two main phases, Feature extraction using DNN and ANN search, which we discuss later in detail. The whole process is done incrementally by scanning one image at a time. Each image is passed to the DNN for feature extraction, and a feature vector is produced for similarity search. Then, we load existing features from the feature database, which are indexed using the Hierarchical Layered Graph (HLG) for faster search processing. Next, an ANN searching method is applied to search for the most similar image features w.r.t the query feature. During the ANN Search using HLG, we retrieve the most similar image feature from the feature database to an incoming query image feature. The incoming query image redundancy status is decided based on some evaluation metrics (Discussed in Section III-C). The metrics threshold can be varied to decide an image's redundancy scale. For example, suppose the similarity threshold value is set to 80%. In that case, any existing features in the database matching 80% with the incoming query feature will be discarded for saving consideration in the database. Setting a low similarity threshold restricts the number of saved
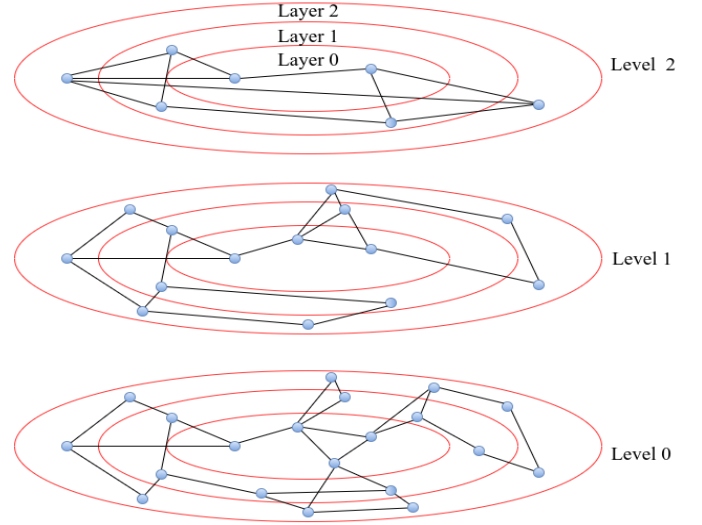

Fig. 3. Illustration of a Hierarchical Layered Graph (HLG) indexing. Each feature vector connects to its M-Nearest Neighbor within the same layer and 1-Nearest Neighbor in the next layers.

features and increases the True Positive rate (TP) in the feature database.

A. Feature extraction with Deep Neural Network (DNN)

The first step toward eliminating data redundancy in the crowd-sensing setting is efficiently representing the data. From the data set section as we can see that the input data in our pipeline is images. A very common method of representing image data is in vector format. Many methods are devised to represent the image data in vector format; using DNN to extract feature vectors is the most popular. The success of DNNs for feature extraction is mainly due to the availability of the data and the computational power. Based on the previous success of DNNs [2] for object detection in images, we have chosen to use ResNet50 architecture for generating feature vectors for the image data. From Figure 2, it can be seen that the ResNet50 model is built upon many Convolution(Conv) blocks stacked one after one. The first seven blocks in the ResNet50 network are Convolutional (Conv) blocks with 64 channel outputs and only one stride at the beginning. Then Next block starts with a Conv block with a stride of 2 and an output channel of 128. This CNN fashion follows onward with 256 and 512 output channels. Next, we perform average pooling on the last Conv layer output. Finally, we feed the output from the average pool into Multi-layered perceptions (MLPs) and save the output from this layer as a feature in our database in 512 lengths of a vector.

B. Approximate Nearest Neighbor (ANN) search using Hierarchical Layered Graph (HLG)

a) ***Index building****:* Fig. 3 illustrates the index structure of our proposed Hierarchical Layered Graph (HLG) approach. Hierarchical Layered Graph (HLG) first arranges all feature vectors in a hierarchical level where the higher level contains

fewer feature vectors and the lower level contains more feature vectors. A probability function, $P(L_v) = F(L_v, l_m)$, is used to determine the level of insertion of an element. The value L_v denotes the level at which an element will be inserted. The probability function normalized by the "level multiplier" l_m, where $l_m=0$ indicates that vectors are only inserted in level 0, gives the probability of a vector insertion in a given level. We achieve the highest performance when we reduce the overlap of shared neighbors between levels. We can reduce overlap by decreasing l_m. However, doing so, as more vectors are moved to the level 0, increases the average number of search traversals. After generating the levels, the Hierarchical Layered Graph (HLG) arranges the feature vectors in layers based on their distances from the centroid, where layer 0 contains the feature vectors that appear to be closer to the centroid and layer L contains the feature vectors that are the farthest from the centroid. The bidirectional graph is constructed by connecting each feature vector to its M-Nearest Neighbor within the same layer and 1-Nearest Neighbor in the next layers. Therefore, the feature vectors of layer $0, 1, 2, ..., L$ will have $M + L - 1, M + L - 2, ..., M$ neighboring nodes in the final graph. The value of M is responsible for the index size and recall. Typically, the optimal value of M ranges from 5 to 48 where a larger value of M leads to a larger index size and higher recall.

*b) k-**Nearest Neighbor (k-NN) retrival**:* Fig. 4 shows the k-NN retrival approach of our proposed Hierarchical Layered Graph (HLG) approach. The search within an index starts with a random point at the upper level where the edges are the longest, and then a greedy search is used within that level until it reaches a local optimum (Fig. 4). The search then switches to the lower level, where the edges are shorter. This time, the starting point is the previous local optimum, and this process continues until the query is reached and the top k-NN to the top k is returned. Layering helps the Hierarchical Layered Graph (HLG) avoid visiting all neighboring nodes within the same layer if the query is in a different layer in the feature space. Moreover, the Hierarchical Layered Graph (HLG) search skips visiting nodes in layers as well if the current node and query are some layers apart from each other in the feature space (Algorithm 3 Line 4).

The index construction outlined in the Algorithm 1 has two phases: (1) building a hierarchical level of proximity graphs within the same layer and (2) adding next-layer connections. The exponential decaying probability distribution $(\lfloor -log_2(unif(0, ..., 1) \times m_l) \rfloor)$ determines the maximum level for each element, where m_l is $\frac{1}{log_2(M)}$. Therefore, the maximum number of levels in the hierarchical graph can be controlled by the maximum established connection parameter M. The insertion process begins at the top level and traverses the graph greedily to locate the closest $cand$ neighbors of the inserted element x. The process is then repeated utilizing the closest neighbors obtained in the previous level as entry points for the algorithm to carry on with the search from the subsequent level. The greedy search algorithm in Algorithm 3 is used to find the closest neighbors, which we discuss later in this section.

Algorithm 1: BUILD$(HLG, X, M, cand, f)$

Input: hierarchical layered graph *HLG*, data vector *X*, number of established connections *M*, size of dynamic candidate list *cand*, outlier filtering factor *f*

Output: Update Hierarchical Layered Graph (HLG) inserting all elements

1   $graph \leftarrow \phi$
2   **foreach** x *of X* **do**
3     $graph \leftarrow$ ADD$(x, M, cand)$
4   **end**
5   $layeredElem \leftarrow$ LAYERING (X, M, f) //Algorithm 2
6   **foreach** $layer$ *of* $layeredElem$ **do**
7     $clg \leftarrow$ get the graph for $layer$
8     $nlg \leftarrow$ get the graph for $(layer + 1)$
9   **foreach** $elem$ *of* $layer$ **do**
10      $n \leftarrow$ SEARCH$(nlg, elem, k = 1, cand = 1)$
11   update $graph$ inserting n to neighbor list of $elem$
12   **end**
13   **end**

In the next phase of index construction, we determine the layers of each element based on their distances from the centroid (Algorithm 2). The control parameter f is used as an outlier filtering factor during the layer determination process. Elements that are f standard deviations from the mean distance do not participate in the layer determination process. The outlier filtering factor f ensures the outliers do not drag the layer boundaries toward them. Next, we extract the graphs for each layer from the previously constructed network. For each inner layer, we identify the closest nearest neighbor in the subsequent layers using the greedy search algorithm (Algorithm 3). Finally, we update the previous network by adding the closest neighbor found in the subsequent layers.

The greedy search process (Algorithm 3) starts at the top level with the entry point ep of the input network and extracts the closest neighboring point p to the incoming query q at that level. Then the search switches to the next lower level and starts with the previous local optimum p, and this process continues until the second lowest level. At the bottom level of the network, g, the algorithm extracts the list of neighbors $cand$ from p and returns the closest neighbors k to q based on their distances.

Search complexity Each Hierarchical Layered Graph (HLG) index level is built as a navigable small-world graph, allowing the greedy search path's hop count to scale logarithmically. Hierarchical Layered Graph (HLG) indexing builds the graph with a set maximum number of links for each element, ensuring a consistent average degree for each element at a certain level. The number of hops and the average degree of the items on the greedy path is multiplied to get the overall amount of distance calculations. As a result, each level of
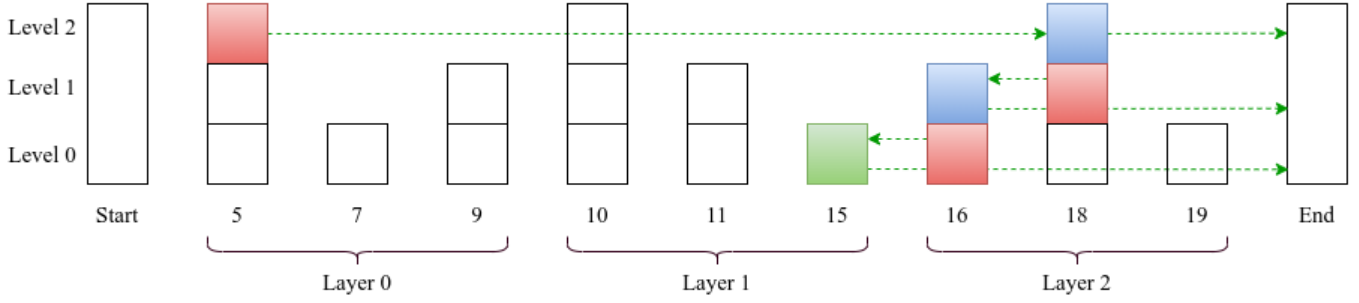
Fig. 4. Illustration of a Hierarchical Layered Graph (HLG) retrieval. Red denotes the starting point in each level, blue denotes the local optimum in each level, and green arrows show the direction of the greedy algorithm to the query(shown green).

Algorithm 2: LAYERING (X, M, f)

Input: data vector X, number of established connections M, outlier filtering factor f

Output: Dictionary of elements with their designated layer

1 $numLayer \leftarrow \log_2 M$
2 $cen \leftarrow$ mean of X
3 $dist \leftarrow$ distances from centroid to all data vectors
4 $avg \leftarrow$ mean of all distances
5 $\sigma \leftarrow$ standard deviation of all distances
6 $u_b \leftarrow avg + f \times \sigma$
7 $l_b \leftarrow$ smallest of $dist$
8 $r \leftarrow \frac{u_b - l_b}{numLayer}$
9 $layeredElem \leftarrow \phi$
10 **foreach** (d, x) *of* $(dist, X)$ **do**
11      $l \leftarrow \frac{d}{r}$
12   add element x to layer l in $layeredElem$
13 **end**
14 **return** $layeredElem$

Algorithm 3: SEARCH$(g, q, k, cand)$

Input: graph index *g*, query element *q*, number of nearest neighbors *k*, size of dynamic candidate list *cand*

Output: *k* closest neighbors to *q*

1 $ep \leftarrow$ get entry point of *g*
2 $L \leftarrow$ get highest level of *g*
3 **for** $l \in L, L - 1, \ldots, 2$ *of g* **do**
4      $p \leftarrow$ extract nearest neighbor to *q* starting with *ep*
5      $ep \leftarrow p$
6 **end**
7 $C \leftarrow$ extract *cand* neighbors to *p* at bottom level of *g*
8 $neighbors \leftarrow$ top *k* closest from *C* to *q*
9 **return** neighbors

---

the Hierarchical Layered Graph (HLG) has logarithmic search complexity. At any given level l with N_l elements, the search complexity is $O(log(N_l))$, where N_l increases from the top to the bottom. The maximum number of elements allowed at the bottom level is N. Therefore, the general search complexity of the Hierarchical Layered Graph (HLG) is determined by $O(log(N))$.

Index building complexity The Hierarchical Layered Graph (HLG) index is constructed in two steps. In the first step, each element is added one at a time by iterative insertions, simply a series of ANN searches at different levels. Thus, the first phase has a complexity of $O(N.log(N))$. The second phase of Hierarchical Layered Graph (HLG) index building is also a series of ANN searches at different layers. Thus, similar to the first phase, the second phase has a complexity of $O(N.log(N))$. Therefore, the overall complexity of the index building of the Hierarchical Layered Graph (HLG) scales as $O(N.log(N))$.

C. Similarity Metrics

We have used two different measurement techniques to evaluate our proposed de-duplication method. As with other previous works, we use traditional Euclidian distance-based similarity search. Moreover, we use cosine similarities as an efficient way of similarity finding among feature vectors leveraging the idea from contrastive learning [11].

Normalized cosine similarity: is a simple process of measuring pair-to-pair relationships based on the similarities between different pairs, such as query-negative samples. We leverage the idea of feature discrimination calculation using cosine similarities from contrastive learning and integrate it into our pipeline for similarity calculation. Many versions of contrastive learning are available for feature representation learning [12], [30], [41]. Previous works [3], [16] used cosine similarity with Informative Noise Contrastive Estimation (InfoNCE) [30] and successfully discriminated vectors in feature space. Motivated by this, we also use the normalized cosine similarity because of its simplicity and faster finding of dissimilarities between features.

$$sim(u, v) = u^T / (||u|| * ||v||) \tag{1}$$

$$x = x / max(||x||_p, \epsilon) \tag{2}$$

The formula for calculating the normalized cosine similarity score is presented in Eq. 1. Here, *Query* is the feature
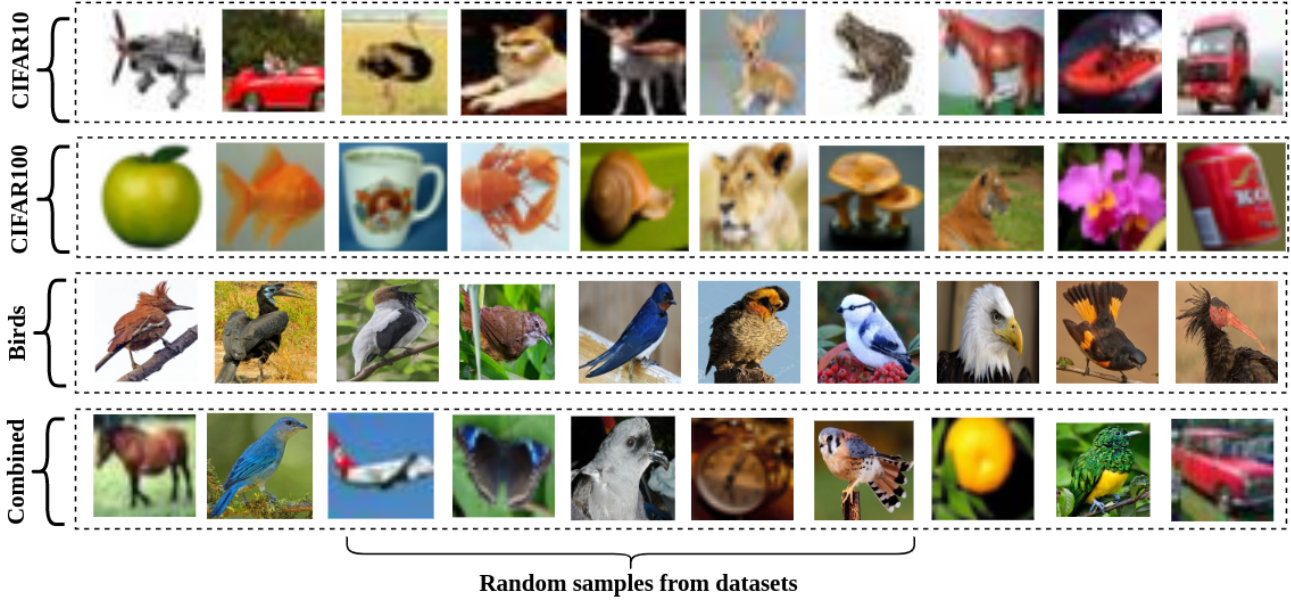
Fig. 5. Illustration of class diversity across experimental data sets.

vector from the query image. On the other hand, *Negative* features are all the other feature vectors saved in the server database. Before performing the cosine similarity calculation, we normalize any vector x using Eq. 2. The Eq. 1 captures the similarity of two features, u and v. The output ranges from 0 to 1, where 0 denotes no similarity and 1 denotes very high similarity.

Distance Based similarity: We have also used Euclidean distance for quantifying the similarity between the query image vector and all other vectors saved in the data set. This method is standard and has successfully calculated similarities in high-dimensional feature space over the years. It calculates a straight-line distance between two points, considering the differences along each dimension and determining the variance between vectors. For example, if $u = (x_1, y_1, z_1, \ldots, n_1)$ and $v = (x_2, y_2, z_2, \ldots, n_2)$ is considered two image feature vector then we can calculate the distance/dissimilarity between them as below Eq. 3:

$$dist(u,v) = \sqrt{(x_2 - x_1)^2 + (y_2 - y_1)^2 + \ldots + (n_2 - n_1)^2}$$
(3)

However, euclidean distance metrics fail when all the feature dimensions do not carry equally valued information, and normalization or feature scaling might be required in this scenario. Due to this reason, our paper does not rely on single performance metrics; instead, uses normalized cosine similarity to verify the correctness of the deduplication process.

IV. DATA SET

To evaluate the performance of our proposed EVIREC method, we have used two publicly available data sets, CIFAR10 and CIFAR100 [20], and one crowd-sensing data set

TABLE I
EXPERIMENTAL DATA SET FOR IMAGE DEDUPLICATION.

Data	Number of images	Size (MB)	Number of classes
CIFAR10 [21]	50,000	47.4	10
CIFAR100 [22]	50,000	114.2	100
Birds	70,626	1600	450
Combined	170,626	1761.6	560

collected from *iNaturalist* [13] online database. Each data set comes with various classes showing the data set's diversity.

CIFAR10: Our first experimental data set is a very well-known benchmark data set *CIFAR10*, for computer vision tasks. There are a total of 60,000 color images in the data set, each of which is a 32×32 pixel resolution. The data set is divided into ten classes, each containing 6,000 images. The classes include common objects such as airplanes, automobiles, birds, cats, deer, dogs, frogs, horses, ships, and trucks. The examples from different classes are illustrated in Figure 5. We split the data set into train and test sets. The train set contains 50,000 images, and the test set contains 10,000 images, where all classes are equally distributed.

CIFAR100: The CIFAR-100 data set is a widely used benchmark data set in data deduplication. CIFAR-100 consists of 100 classes, with each class containing 600 images. Moreover, these categories are divided into 20 superclasses, each containing five classes. The superclasses capture higher-level semantic information, while the individual classes represent specific objects or characteristics. The data set contains 50,000 training and 10,000 test images, equally distributed across different classes. Each color image in CIFAR-100 has a 32×32 pixels resolution. We choose this data set due to its challenges from relatively low-resolution images and the presence of fine-

grained classes. The data set contains the hierarchy of super-class and sub-classes as shown in Figure 5. Deduplication becomes harder as many classes share visual similarities, requiring models to learn subtle discriminative features.

iNaturalist-Birds: Our last experimental data set is from the iNaturalist. The iNaturalist Birds data set is a comprehensive collection of bird species images prepared for bird classification and identification. It is derived from the iNaturalist platform, a popular online community for nature enthusiasts to share observations and photographs of various species. The iNaturalist Birds data set contains over 70,000 bird images covering many species worldwide. We have chosen 450 different bird classes with equal distribution for the de-duplication task. The inter-class similarities and intra-class dissimilarities make the data set perfect (See Figure 5) for exploring de-duplication tasks. We have 73,776 color images in the data set, with dimensions of 224×224 pixels. The training set contains 70626 images, and we perform the deduplication task on the training set for each method.

Combined data set: To verify the robustness of the designed pipeline, we created a combined data set that introduced challenges from three of our benchmark data sets. Using this data set, we investigate the performance of our proposed pipeline by comparing different SOTA methods when a very high and diverging amount of classes is introduced. Table I shows that our combined data set consists of 170,626 images and holds 560 classes. The class diversity of the combined data set is presented in Figure 5.

TABLE II
NOTATION TABLE.

Symbol	Description
Th_d	Euclidean distance threshold
Th_s	Cosine similarity threshold
Dup	Number of duplicate or near duplicate images
δ_s	Database size reduction in megabytes
ξ	Percentage of redundancy elimination
R_t	Number of redundant images in the data set

V. Experiment

We compare the performance of our EVIREC methods with hashing-based methods and CNN-based methods. The evaluation is conducted using three metrics:

Number of duplicates found (Dup): This metric measures the ability of each method to identify and detect duplicate images within a data set. Duplicate images refer to multiple copies or instances of the same image. The higher the number of duplicates found, the better the method's performance in identifying and flagging redundant images.

Database size reduction in megabytes (δ_s): This metric quantifies the reduction in storage space achieved by applying each method to the data set. It measures the difference in the size of the original data set and the size of the data set after applying the method. A larger reduction in database size indicates better efficiency in terms of storage requirements.

TABLE III
DE-DUPLICATION RESULTS ON THE CIFAR10 DATA SET WITH 50000 IMAGES AND TOTAL SIZE OF 47.4 MB.

Method	Th_d	Dup	δ_s	ξ
PHash	10	2292	1.97	4.58%
PHash	15	22128	19.26	44.26%
PHash	20	48985	43.00	97.99%
DHash	10	2088	1.81	4.17%
DHash	15	27874	24.37	55.75%
DHash	20	48541	42.61	97.10%
WHash	10	31260	27.18	62.53%
WHash	15	44297	38.78	88.61%
WHash	20	49617	43.56	99.25%
AHash	10	29722	25.81	59.45%
AHash	15	45458	39.82	90.93%
AHash	20	49509	43.46	99.04%
EVIREC	10	44297	38.78	88.61%
EVIREC	15	49235	46.71	98.49%
EVIREC	**20**	**49857**	**47.27**	**99.73%**

Percentage of redundancy elimination (ξ): This metric assesses how much each method eliminates redundancy within the data set. Redundant images provide no additional information compared to other images in the data set. The percentage of redundancy elimination is calculated using the equation referenced as Eq. 4, where R_t represents the total number of redundant images in the data set.

To calculate the percentage of redundancy elimination, the total number of images in the data set is subtracted from the number of classes in that data set. This subtraction yields the number of redundant images, as classes represent unique categories, and any additional instances of images within the same class are considered redundant. Consequently, the optimal number of unique images in any data set equals the number of classes present in that data set.

Overall, the comparisons aim to evaluate the performance of EVIREC method in terms of its ability to identify duplicates, reduce database size, and eliminate redundancy compared to other hashing-based and CNN-based methods. The metrics provide quantitative measures to assess the effectiveness of each method, and the percentage of redundancy elimination specifically highlights the value of unique images within a data set based on the number of classes. All the useful notations in this section are enlisted in Table II.

$$\xi = \frac{Dup}{R_t} \times 100\% \qquad (4)$$

A. Comparison with hashing-based methods

We conduct a comparative analysis of our EVIREC method against four state-of-the-art hashing-based methods, namely WHash [34], PHash [42], DHash [38] and AHash [4] for the image deduplication task. To evaluate each method, we apply three different distance thresholds ($Th_d = [10, 15, 20]$) to experimental data sets. The performance of the comparing

Method	Th_d	Dup	δ_s	ξ
PHash	10	1817	3.63	3.64%
PHash	15	19811	41.36	39.70%
PHash	20	48933	104.11	98.06%
DHash	10	4313	8.46	8.64%
DHash	15	30517	63.96	61.15%
DHash	20	48650	103.42	97.49%
WHash	10	31494	64.98	63.11%
WHash	15	43975	92.64	88.12%
WHash	20	49547	105.33	99.29%
AHash	10	29818	61.61	59.75%
AHash	15	45063	95.12	90.30%
AHash	20	49458	105.13	99.11%
EVIREC	10	43993	92.65	88.13%
EVIREC	15	49551	105.34	99.30%
EVIREC	**20**	**49744**	**114.07**	**99.69%**

TABLE IV
DE-DUPLICATION RESULTS ON THE CIFAR100 DATA SET WITH 50000
IMAGES AND TOTAL SIZE OF 114.2 MB.

methods on CIFAR10, CIFAR100, and Birds data sets is presented in Table III, Table IV, and Table V, respectively.

TABLE V
DE-DUPLICATION RESULTS ON THE BIRDS DATA SET WITH 70626 IMAGES
AND TOTAL SIZE OF 1600 MB.

Method	Th_d	Dup	δ_s	ξ
PHash	10	5826	120.38	8.30%
PHash	15	37365	787.56	53.24%
PHash	20	69558	1490.6	99.11%
DHash	10	3683	77.26	5.24%
DHash	15	44437	945.54	63.32%
DHash	20	69123	1481.51	98.50%
WHash	10	34716	727.45	49.47%
WHash	15	59241	1261.10	84.42%
WHash	20	70002	1500.12	99.75%
AHash	10	33244	692.34	47.37%
AHash	15	61781	1317.24	88.03%
AHash	20	69839	1496.70	99.52%
EVIREC	10	59241	1261.10	84.42%
EVIREC	15	68495	1550.3	97.60%
EVIREC	**20**	**69982**	**1554.7**	**99.81%**

The results from the experiment conducted on CIFAR10 (see Table III) demonstrate that EVIREC successfully identifies 49,857 duplicate images out of a total of 49,990 images, resulting in a redundancy elimination rate of 99.73% when using a distance threshold of $Th_d = 20$. Moreover, EVIREC effectively reduces the size of the database by 47.27 megabytes, compared to the original size of 47.4 megabytes. WHash, a competing method, achieves similar results to EVIREC by detecting 49,857 duplicate images, leading to a redundancy elimination rate of 99.25% and reducing the database size by 43.56 megabytes. On the other hand, PHash, DHash, and AHash demonstrate redundancy elimination rates of 97.99%, 97.10%, and 99.04%, respectively.

TABLE VI
DE-DUPLICATION RESULTS ON THE COMBINED DATA SET WITH 170626
IMAGES AND TOTAL SIZE OF 1761.6 MB.

Method	Th_d	Dup	δ_s	ξ
PHash	10	13582	155.14	7.98%
PHash	15	107545	1079.46	63.23%
PHash	20	169313	1654.46	99.55%
DHash	10	13950	117.67	8.2%
DHash	15	126727	1229.88	74.51%
DHash	20	168766	1647.72	99.23%
WHash	10	110299	933.22	64.85%
WHash	15	155137	1457.84	91.22%
WHash	20	169657	1709.21	99.76%
AHash	10	105272	886.80	61.90%
AHash	15	159273	1483.17	93.65%
AHash	20	169606	1703.14	99.73%
EVIREC	10	150015	1421.59	88.21%
EVIREC	15	169912	1721.71	99.91%
EVIREC	**20**	**169963**	**1724.4**	**99.94%**

TABLE VII
DE-DUPLICATION RESULTS ON THE CIFAR10 DATA SET WITH 50000
IMAGES AND TOTAL SIZE OF 47.4 MB.

Method	Th_s	Dup	δ_s	ξ
CEDedup	0.85	8638	7.59	17.27%
CEDedup	0.90	1864	1.64	3.73%
CEDedup	0.95	297	0.26	0.59%
EVIREC	**0.85**	**49988**	**47.39**	**99.99%**
EVIREC	0.90	49944	46.35	99.90%
EVIREC	0.95	47957	42.35	96.11%

When considering other distance thresholds, EVIREC outperforms the hashing-based methods in Table III. The same trend is observed for the CIFAR100 data set, as shown in Table IV, where EVIREC successfully detects 49,744 duplicate images, resulting in a redundancy elimination rate of 99.69%. This leads to a reduction in the database size by 114.07 megabytes out of the original 114.2 megabytes. Additionally, Table V illustrates the effectiveness of EVIREC on the Birds data set, detecting 69,982 duplicate images and achieving a redundancy elimination rate of 99.81%. This results in a database size reduction of 1554.7 megabytes out of the original 1600 megabytes.

The experimental results for the comparing methods on the combined data set are presented in Table VI. Despite the diverse range of object sizes, shapes, and camera angles within the combined data set, EVIREC demonstrates its exceptional performance by successfully detecting 169,963 redundant images, resulting in an impressive redundancy elimination rate of 99.94% for threshold distance 20. In Table VI, EVIREC outperforms all other comparing methods for all the corresponding threshold distances. Additionally, EVIREC achieves a significant reduction in database size, reducing it by 1724.4 megabytes compared to the original size of 1761.6 megabytes.

B. Comparison with CNN-based methods

We have compared our EVIREC method and the state-of-the-art CNN-based method CE-Dedup [24]. Our method's performance was evaluated based on the cosine similarity threshold. The experimental results for CIFAR10, CIFAR100, and the Birds data set are presented in Table VII, Table VIII, and Table IX respectively, considering three different similarity thresholds ($Th_s = [0.85, 0.90, 0.95]$).

TABLE VIII
DEDUPLICATION RESULTS ON THE CIFAR100 DATA SET WITH 50000 IMAGES AND TOTAL SIZE OF 114.2 MB.

Method	Th_s	Dup	δ_s	ξ
CEDedup	0.85	9389	19.39	18.81%
CEDedup	0.90	3224	6.56	6.46%
CEDedup	0.95	941	1.97	1.88%
EVIREC	**0.85**	**49887**	**114.02**	**99.97%**
EVIREC	0.90	49835	113.85	99.87%
EVIREC	0.95	47519	105.45	95.23%

TABLE IX
DEDUPLICATION RESULTS ON THE BIRDS DATA SET WITH 70626 IMAGES AND TOTAL SIZE OF 1600 MB.

Method	Th_s	Dup	δ_s	ξ
CEDedup	0.85	46291	984.00	65.96%
CEDedup	0.90	18447	389.72	26.28%
CEDedup	0.95	4769	103.75	6.79%
EVIREC	**0.85**	**68587**	**1554.3**	**97.73%**
EVIREC	0.90	67968	1539.9	96.85%
EVIREC	0.95	67849	1537.5	96.68%

TABLE X
DEDUPLICATION RESULTS ON THE COMBINED DATA SET WITH 170626 IMAGES AND TOTAL SIZE OF 1761.6 MB.

Method	Th_s	Dup	δ_s	ξ
CEDedup	0.85	105272	886.80	61.90%
CEDedup	0.90	33244	692.34	47.37%
CEDedup	0.95	3683	77.26	5.24%
EVIREC	**0.85**	**167566**	**1589.35**	**98.53%**
EVIREC	0.90	163484	1521.84	96.13%
EVIREC	0.95	159274	1483.19	93.65%

Across all four data sets and corresponding similarity thresholds, EVIREC consistently outperforms CE-Dedup. For the CIFAR10 data set, EVIREC successfully detects 49,988 duplicate images out of a total of 49,990 images, resulting in a redundancy elimination rate of 99.99% and reducing the database size by 47.39 megabytes out of the original 47.4 megabytes for $Th_s = 0.85$ (Table VII). In contrast, CE-Dedup only identifies 8,638 duplicate images out of 49,990, achieving a redundancy elimination rate of 17.27% and reducing the database size by 7.59 megabytes for the same similarity threshold (Table VII). Similar trends can be observed in Table VIII for the CIFAR100 data set and Table IX for the Birds data set. CE-Dedup eliminates 65.96% of redundant images

in the Birds data set, while EVIREC achieves a significantly higher redundancy elimination rate of 97.73% (Table IX).

The experimental results for comparing methods are presented in Table X, showcasing the performance on the combined data set. Despite the diverse range of object sizes, shapes, and camera angles within the combined data set, EVIREC demonstrates its effectiveness by successfully detecting 167,566 redundant images, resulting in a remarkable redundancy elimination rate of 98.53%. In comparison to CE-Dedup, as depicted in Table X, EVIREC surpasses it across all corresponding similarity thresholds. Furthermore, EVIREC achieves a substantial reduction in database size, reducing it by 1589.35 megabytes compared to the original size of 1761.6 megabytes.

Based on the experimental results, it is evident that EVIREC consistently outperforms CE-Dedup across all four data sets (Table VII, VIII, IX, X). Therefore, EVIREC has proven to be the most robust method for the image deduplication task compared to state-of-the-art hashing-based and CNN-based methods.

C. Ablation Study

In this section, we first perform an ablation study on each data set and evaluation metrics to demonstrate the effectiveness of our proposed model. Next, we perform an ablation study on each important hyper-parameters, such as distance threshold and similarity threshold; the summary of the ablation study is illustrated in Table XI.

The main goal of the deduplication method is to reduce the redundant data in the database while increasing the True Positive (TP) rate throughout the process. The rate of TP is directly connected to the threshold we design for the deduplication purpose. For example, Suppose we choose to use cosine similarity as the evaluation metric. In that case, a lower threshold will discard the query image if it slightly matches any image stored in the database. Thus It will increase the TP and restrict more images to be stored in the database. On the contrary, a higher threshold will allow more query images to pass through the process and consequently increase False Negative in the database. As shown in Table XI, increasing the threshold increase duplicates for *Bird Class: Brown Creeper* from 7 to 16. Figure 6 shows the query Vs. Duplicate images that are stored in the database based on different similarity thresholds. Suppose we compare the different rows in 6. In that case, duplicates are more similar to the query image when using a higher similarity threshold in deduplication.

Using distance metrics for the deduplication process works the opposite of similarity metrics. Here, a higher distance threshold filters more duplicates as they are distant in the feature space. So, a higher threshold gives a higher True Positive and reduces the redundancy in the database. Table XI presents the number of duplicates stored against different distance thresholds for *Bird Class: Brown Creeper*. We see that the number of duplicates increases from 8 to 45 due to easing the distance threshold from 20 to 15. The above study shows that our normalized cosine similarity metrics achieve a

TABLE XI

ABLATION STUDY FOR THE NUMBER OF DUPLICATES STORED FOR BIRD CLASS: BROWN CREEPER BASED ON DIFFERENT METRICS AND THRESHOLDS.

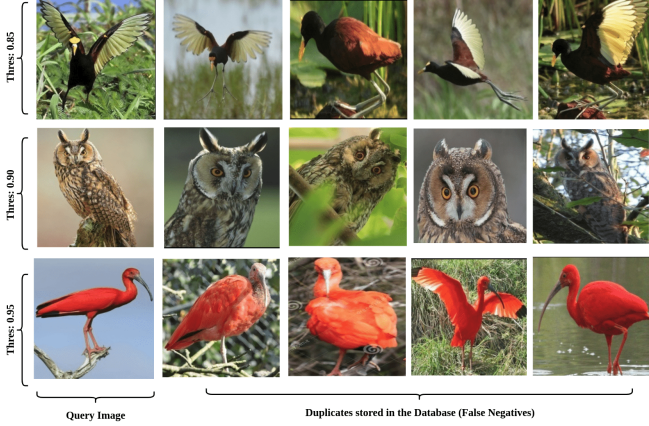| Metrics	Threshold	Num. of Duplicates
Cosine Similarity	0.85	7
	0.90	12
	0.95	16
Euclidean Distance	10	45
	15	33
	20	8

Fig. 6. Ablation Study: Illustration of False Negatives with Cosine Similarity as evaluation metrics.
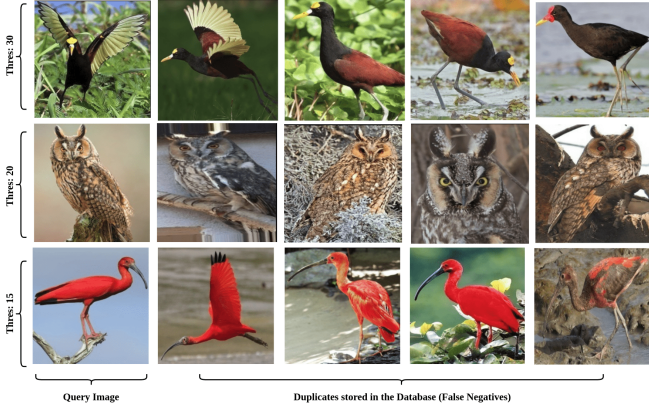

Fig. 7. Ablation Study: Illustration of False Negatives with Euclidean Distance as evaluation metrics.

higher true positive rate than the Euclidean distance metrics. Moreover, duplicates in Figure 7 are more similar to their query image compared to Figure 6 due to the higher number of duplicates allowed by the Euclidean distance metrics.

VI. CONCLUSION

Visual crowd-sensing (VCS) asks users to contribute to different tasks by sending images or video information from their surroundings. Due to the abundance of participant data, it is hard to identify and eliminate redundant images. Visual crowd-sensing provides a more informative and diverse image database. Our proposed Efficient Visual Indexing and Retrieval for Edge Crowd-sensing (EVIREC) method extracts features from an image database using Deep Neural Network (DNN). It performs Approximate Nearest Neighbor (ANN) search to retrieve similar images. EVIREC then efficiently eliminates the redundant data based on the distant threshold in the feature space. The experimental result shows that EVIREC outperforms state-of-the-art hashing-based and CNN-based methods for the CIFAR10, CIFAR100, and Birds data set by eliminating redundant images up to 99.99%.

REFERENCES

[1] Ahmed, N., Natarajan, T., Rao, K.R.: Discrete cosine transform. IEEE transactions on Computers **100**(1), 90–93 (1974)

[2] Biswas, D., Rahman, M.M.M., Zong, Z., Tešić, J.: Improving the energy efficiency of real-time dnn object detection via compression, transfer learning, and scale prediction. In: 2022 IEEE International Conference on Networking, Architecture and Storage (NAS). pp. 1–8 (2022). https://doi.org/10.1109/NAS55553.2022.9925528

[3] Biswas, D., Tešić, J.: Progressive domain adaptation with contrastive learning for object detection in the satellite imagery (2023)

[4] Chamoso, P., Rivas, A., Martín-Limorti, J.J., Rodríguez, S.: A hash based image matching algorithm for social networks. In: Trends in Cyber-Physical Multi-Agent Systems. The PAAMS Collection-15th International Conference, PAAMS 2017 15. pp. 183–190. Springer (2018)

[5] Chen, C.C., Hsieh, S.L.: Using binarization and hashing for efficient sift matching. Journal of Visual Communication and Image Representation **30**, 86–93 (2015)

[6] Chen, H., Guo, B., Yu, Z., Chen, L., Ma, X.: A generic framework for constraint-driven data selection in mobile crowd photographing. IEEE Internet of Things Journal **4**(1), 284–296 (2017)

[7] Guo, B., Chen, H., Yu, Z., Nan, W., Xie, X., Zhang, D., Zhou, X.: Taskme: Toward a dynamic and quality-enhanced incentive mechanism for mobile crowd sensing. International Journal of Human-Computer Studies **102**, 14–26 (2017)

[8] Guo, B., Chen, H., Yu, Z., Xie, X., Huangfu, S., Zhang, D.: Fliermeet: a mobile crowdsensing system for cross-space public information reposting, tagging, and sharing. IEEE Transactions on Mobile Computing **14**(10), 2020–2033 (2014)

[9] Guo, B., Han, Q., Chen, H., Shangguan, L., Zhou, Z., Yu, Z.: The emergence of visual crowdsensing: Challenges and opportunities. IEEE Communications Surveys & Tutorials **19**(4), 2526–2543 (2017)

[10] Guo, B., Wang, Z., Yu, Z., Wang, Y., Yen, N.Y., Huang, R., Zhou, X.: Mobile crowd sensing and computing: The review of an emerging human-powered sensing paradigm. ACM computing surveys (CSUR) **48**(1), 1–31 (2015)

[11] Hadsell, R., Chopra, S., LeCun, Y.: Dimensionality reduction by learning an invariant mapping. In: 2006 IEEE Computer Society Conference on Computer Vision and Pattern Recognition (CVPR'06). vol. 2, pp. 1735–1742. IEEE (2006)

[12] Hjelm, R.D., Fedorov, A., Lavoie-Marchildon, S., Grewal, K., Bachman, P., Trischler, A., Bengio, Y.: Learning deep representations by mutual information estimation and maximization. arXiv preprint arXiv:1808.06670 (2018)

[13] iNaturalist: inaturalist is a joint initiative of the california academy of sciences and the national geographic society. (December 2022), https://www.inaturalist.org/observations

[14] Jiang, Y., Xu, X., Terlecky, P., Abdelzaher, T., Bar-Noy, A., Govindan, R.: Mediascope: selective on-demand media retrieval from mobile devices. In: Proceedings of the 12th international conference on Information processing in sensor networks. pp. 289–300 (2013)

[15] Johnson, J., Douze, M., Jégou, H.: Billion-scale similarity search with gpus. IEEE Transactions on Big Data **7**(3), 535–547 (2019)

[16] Kang, G., Jiang, L., Yang, Y., Hauptmann, A.G.: Contrastive adaptation network for unsupervised domain adaptation. In: Proceedings of the IEEE/CVF conference on computer vision and pattern recognition. pp. 4893–4902 (2019)

[17] Kaur, R., Bhattacharya, J., Chana, I.: Deep cnn based online image deduplication technique for cloud storage system. Multimedia Tools and Applications **81**(28), 40793–40826 (2022)

[18] Kim, S., Robson, C., Zimmerman, T., Pierce, J., Haber, E.M.: Creek watch: pairing usefulness and usability for successful citizen science. In: Proceedings of the SIGCHI conference on human factors in computing systems. pp. 2125–2134 (2011)

[19] Kouiroukidis, N., Evangelidis, G.: The effects of dimensionality curse in high dimensional knn search. In: 2011 15th Panhellenic Conference on Informatics. pp. 41–45. IEEE (2011)

[20] Krizhevsky, A., Hinton, G., et al.: Learning multiple layers of features from tiny images (2009)

[21] Krizhevsky, A., Nair, V., Hinton, G.: Cifar-10 (canadian institute for advanced research) http://www.cs.toronto.edu/ kriz/cifar.html

[22] Krizhevsky, A., Nair, V., Hinton, G.: Cifar-100 (canadian institute for advanced research) http://www.cs.toronto.edu/ kriz/cifar.html

[23] Li, J., Qian, X., Li, Q., Zhao, Y., Wang, L., Tang, Y.Y.: Mining near duplicate image groups. Multimedia Tools and Applications **74**(2), 655–669 (2015)

[24] Li, X., Chang, L., Liu, X.: Ce-dedup: Cost-effective convolutional neural nets training based on image deduplication. In: 2021 IEEE Intl Conf on Parallel & Distributed Processing with Applications, Big Data & Cloud Computing, Sustainable Computing & Communications, Social Computing & Networking (ISPA/BDCloud/SocialCom/SustainCom). pp. 11–18. IEEE (2021)

[25] Li, X., Chang, L., Liu, X.: Qhash: An efficient hashing algorithm for low-variance image deduplication. In: 2021 IEEE 23rd Int Conf on High Performance Computing & Communications; 7th Int Conf on Data Science & Systems; 19th Int Conf on Smart City; 7th Int Conf on Dependability in Sensor, Cloud & Big Data Systems & Application (HPCC/DSS/SmartCity/DependSys). pp. 9–15. IEEE (2021)

[26] Ma, H., Zhao, D., Yuan, P.: Opportunities in mobile crowd sensing. IEEE Communications Magazine **52**(8), 29–35 (2014)

[27] Mahabubur Rahman, M.M., Tešić, J.: Hybrid approximate nearest neighbor indexing and search (hannis) for large descriptor databases. In: 2022 IEEE International Conference on Big Data (Big Data). pp. 3895–3902 (2022). https://doi.org/10.1109/BigData55660.2022.10020464

[28] Malkov, Y.A., Yashunin, D.A.: Efficient and robust approximate nearest neighbor search using hierarchical navigable small world graphs. IEEE transactions on pattern analysis and machine intelligence **42**(4), 824–836 (2018)

[29] Nbt, Y., Ismail, A., Majid, N.: Deduplication image middleware detection comparison in standalone cloud database. Int J Adv Comput Sci Technol (IJACST) **5**(3), 12–18 (2016)

[30] Oord, A.v.d., Li, Y., Vinyals, O.: Representation learning with contrastive predictive coding. arXiv preprint arXiv:1807.03748 (2018)

[31] Rahman, M.M.M., Tešić, J.: Evaluating hybrid approximate nearest neighbor indexing and search (hannis) for high-dimensional image feature search. In: 2022 IEEE International Conference on Big Data (Big Data). pp. 6802–6804 (2022). https://doi.org/10.1109/BigData55660.2022.10021048

[32] Saini, M.K., Gadde, R., Yan, S., Ooi, W.T.: Movimash: online mobile video mashup. In: Proceedings of the 20th ACM international conference on Multimedia. pp. 139–148 (2012)

[33] Shensa, M.J., et al.: The discrete wavelet transform: wedding the a trous and mallat algorithms. IEEE Transactions on signal processing **40**(10), 2464–2482 (1992)

[34] Singh, S.P., Bhatnagar, G.: A robust image hashing based on discrete wavelet transform. In: 2017 IEEE International Conference on Signal and Image Processing Applications (ICSIPA). pp. 440–444. IEEE (2017)

[35] Thaiyalnayaki, S., Sasikala, J., Ponraj, R.: Detecting near-duplicate images using segmented minhash algorithm. International Journal of Advanced Intelligence Paradigms **12**(1-2), 192–206 (2019)

[36] Tuite, K., Snavely, N., Hsiao, D.y., Tabing, N., Popovic, Z.: Photocity: training experts at large-scale image acquisition through a competitive game. In: Proceedings of the SIGCHI Conference on Human Factors in Computing Systems. pp. 1383–1392 (2011)

[37] Uddin, M.Y.S., Wang, H., Saremi, F., Qi, G.J., Abdelzaher, T., Huang, T.: Photonet: a similarity-aware picture delivery service for situation awareness. In: 2011 IEEE 32nd Real-Time Systems Symposium. pp. 317–326. IEEE (2011)

[38] Wang, J., Fu, X., Xiao, F., Tian, C.: Dhash: Enabling dynamic and efficient hash tables. arXiv preprint arXiv:2006.00819 (2020)

[39] White, J., Thompson, C., Turner, H., Dougherty, B., Schmidt, D.C.: Wreckwatch: Automatic traffic accident detection and notification with smartphones. Mobile Networks and Applications **16**(3), 285–303 (2011)

[40] Wu, Y., Mei, T., Xu, Y.Q., Yu, N., Li, S.: Movieup: Automatic mobile video mashup. IEEE Transactions on Circuits and Systems for Video Technology **25**(12), 1941–1954 (2015)

[41] Wu, Z., Xiong, Y., Yu, S.X., Lin, D.: Unsupervised feature learning via non-parametric instance discrimination. In: Proceedings of the IEEE conference on computer vision and pattern recognition. pp. 3733–3742 (2018)

[42] Zauner, C.: Implementation and benchmarking of perceptual image hash functions (2010)